Comparison of Predictions and Experimental Data for Hypersonic Pitching Motion Stability

R. A. East* and G. R. Hutt†
University of Southampton, Hants, England, United Kingdom

The stability of oscillatory motions of vehicles flying at hypersonic Mach numbers is of considerable relevance to their initial design. Methods are needed for quick and accurate predictions of stability and control that are applicable over a wide range of body shapes, angles of attack, and flow conditions without the need to resort to computationally time-consuming numerical flowfield calculation methods. The purpose of this paper is to present experimental and theoretical data concerning the static and dynamic pitching stability of pointed and blunted 10 deg semiangle cones and a double-flared hyperballistic shape. Although Newtonian theory gives inadequate accuracy of prediction, inviscid embedded Newtonian theory, which accounts for the reduced dynamic pressure and lower flow velocity in the embedded flow downstream of the strong bow shock, is shown to provide surprisingly good agreement with experimental data over a wide range of conditions. Comparisons with experimental results show that the broad flow features associated with nose bluntness, angle of attack, and center of gravity position and their effect on static and dynamic stability are well described in regimes not containing flow structural change. However, in some cases discrepancies exist between the predictions and experimental observations, and these have been attributed to a variety of viscous-flow phenomena involving boundary-layer transition and flow separation, including complex lee-surface vortical flows.

Nomenclature

c = reference length, pointed cone length L for cones, cylinder diameter d_N for hyperballistic shapes
C_m = pitching moment coefficient about $C.G.$ $C_m = M_p/\frac{1}{2}\rho_\infty V_\infty^2 Sc$
C_{m_α} = pitching moment slope coefficient, $C_{m_\alpha} = \partial C_m/\partial\alpha$
$C_{m_{\dot\alpha}}$ = pitching moment derivative due to rate of change of angle of attack, $C_{m\alpha} = \partial C_m/\partial(\dot\alpha c/2V_\infty)$
C_{m_q} = pitching moment derivative due to rate of pitching, $C_{m_q} = \partial C_m/\partial(qc/2V_\infty)$
C_p = pressure coefficient, $C_p = (p - p_\infty)/(\frac{1}{2}\rho_\infty V_\infty^2)$
C_{p_o} = blast wave pressure coefficient
C_γ = empirical coefficient
d_B = base diameter
d_N = diameter of hemispherical nose
L = body length, length of equivalent pointed cone for blunt cones
M_∞ = freestream Mach number
M_p = pitching moment, positive nose up
p = pressure
p_∞ = freestream static pressure
q = pitch rate (rads^{-1})
r = body cross-sectional radius, $r' = r/d_N$
Re = Reynolds number per unit length
Re_b = Reynolds number based on cone base diameter d_B
S = reference area, base area ($= \pi d_B^2/4$) for cones
V = velocity in x direction in embedded flow
V_∞ = freestream velocity
v_n = velocity component perpendicular to body element
x_B = x coordinate of body base
x_{cg} = center of gravity position measured from the cone apex
z = vertical coordinate where $z' = z/d_N$
α = angle of attack
γ = ratio of specific heats
ρ = air density
ω = angular velocity
ω' = $\omega c/2V_\infty$, reduced-frequency parameter

Subscripts

N = body nose
S = shock
Newt. = Newtonian value
∞ = freestream

Superscript

= dimensionless distances, e.g., $x' = x/d_N$

Received Oct. 26, 1987; revision received Feb. 15, 1988.

*Professor of Aeronautics and Head of Department of Aeronautics and Astronautics. Member AIAA.

†Lecturer, Department of Aeronautics and Astronautics. Member AIAA.

Introduction

HYPERSONIC vehicle technology is a subject of increasing importance in a variety of applications. Particular applications include future space transportation systems, aeroassisted orbital transfer vehicles, the hypersonic transport, the transatmospheric aircraft, and re-entry vehicles. Broad aspects of vehicle performance are determined by the steady aerodynamic characteristics, but the ability to follow a predetermined flight path or re-entry trajectory is determined by stability and control considerations.

In order that pitch stability of hypersonic vehicles and its influences on design may be explored further, there is a requirement for both an experimental and theoretical data base. Moreover, there is a need for a rapid means of prediction of vehicle stability data that can be validated with experimental results. Modern computational fluid dynamics, applied to unsteady hypersonic flowfields, can be limited in regard to the range of conditions that can be quickly covered. This paper highlights the surprisingly good agreement between the less time-consuming semiempirical inviscid embedded Newtonian technique and experimental data for pitch stability derivatives obtained for a range of axisymmetric models.

The most fundamental approximation of hypersonic pressure coefficients is given by the so-called Newtonian impact technique.[1,2] However, it was noted by Busemann[3] that a centrifugal pressure term must be included with the Newtonian approximation to cater for curved particle trajectories within the shock layer. This resulted in the so-called Newton-Busemann method. The centrifugal effect is necessary for the ideal Newtonian case of an infinitesimally thin shock layer obtained at the gas dynamic limit of $M = \infty$, $\gamma = 1$. Despite this observation of the requirement of a centrifugal term in the gas dynamic limit, it must be noted that for the majority of hypersonic flight vehicles, infinitesimally thin shock layer and $\gamma \to 1$ assumptions are not well satisfied. These limitations and the subsequent effect on the prediction of pressure coefficients in realistic hypersonic flight regimes were considered by Seiff[4] and subsequently Ericsson.[5] The consequences of finite shock-layer thickness and bow shock waves determined by nose shape and drag coefficient led to the semiempirical embedded Newtonian technique. This ignores the centrifugal term, since the theoretical gas dynamic limit is not approached and concentrates on the entropy layer effects downstream of the nose, modifying the velocity and dynamic pressure fields in which the downstream body is embedded. For situations in which the ideal limiting Newtonian case is approached, Tong and Hui[6] have extended the embedded Newtonian method to include the centrifugal correction term in the embedded flow. This paper presents results from all three of the above techniques and draws comparisons with experimental data for pointed and blunted cones and a hyperballistic shape.

A major aerodynamic feature of many of the hypersonic vehicle applications is that the flows are dominated by viscous effects such as viscous interaction, boundary-layer transition, separated flows, and upper-surface vortical flows. These phenomena, which are strongly influenced by vehicle geometry, can exert a large effect on both static and dynamic stability at hypersonic Mach numbers. The effects of these phenomena are exposed by comparing inviscid/viscous hypersonic vehicle pitch stability data obtained over a range of appropriate Reynolds numbers.

Prediction Methods for Three-Dimensional Shapes

The simplest technique for establishing the pressure coefficient on a hypersonic flight vehicle is the Newtonian impact theory. In this flow model, it is assumed that the fluid particles do not interact, and that the only change in the velocity of a particle impinging on a body surface takes place normal to the surface. The normal component of momentum is assumed to be transferred to the body, and the particles continue to move along the surface with zero tangential acceleration. If the velocity component normal to the surface is written as v_n, the Newtonian surface pressure coefficient becomes

$$C_{p_{\text{Newt.}}} = 2\left(\frac{v_n}{V_\infty}\right)^2 \tag{1}$$

A semiempirical modification to the preceding expression replaces the factor 2 by $C_{p_{\max}}$, the pressure coefficient at the stagnation point to the body. Examples of the use of the unsteady Newtonian impact theory to calculate the stability derivatives of cones are given by Tobak and Wehrend.[7]

Busemann[3] observed that the expression given in Eq. (1) strictly applies only at the freestream surface of the Newtonian shock layer, since a normal pressure gradient must exist as a consequence of the curved trajectories followed by the fluid particles in this layer. The body surface pressure in the Newtonian-Busemann theory may therefore be written as

$$P_{\text{surface}} = P_{\text{Newt.}} + P_{\text{cent}} \tag{2}$$

where P_{cent} is the centrifugal pressure correction. For steady flow past bodies whose surface geodesics are straight, $P_{\text{cent}} = 0$, and Eq. (1) provides the appropriate expression for C_p. For bodies with curved geodesics, Cole[8] for slender axisymmetric bodies, and Hui[9] for general two-dimensional and axisymmetric bodies showed that the Newton-Busemann expression [Eq. (2)] could be obtained as the limit of gas dynamic theories for $M_\infty \to \infty$ and $\gamma \to 1$. For nonsteady flow, the particle trajectories do not follow the surface geodesics, although they still move tangentially to the surface. In this case, the curvature of the trajectory is dependent both on the geometric surface curvature and on the curvature of the trajectory induced by the body motion. Mahood and Hui[10] have applied the Newton-Busemann method to unsteady flow past oscillating wedges at zero-mean incidence. For both shapes, the steady centrifugal pressure correction term is zero, but the unsteady correction term is significant. They showed that in the double limit $M_\infty \to \infty$ and $\gamma \to 1$, the resulting Newton-Busemann unsteady pressure was identical to that deduced from gas dynamics theories by Hui[11] for oscillating wedges, and Mahood and Hui[10] for oscillating cones. This observation was important in explaining the apparent anomaly that had existed in the comparison between the simple unsteady Newtonian model and the limits of theories based on the gas equations of motion for very high Mach numbers as, for example, observed by Scott[12] for the case of oscillating cones. A central assumption in the Newtonian flow model is that the shock layer is thin and the shock wave, therefore, lies close to the body surface. This is often closely satisfied for wedges and cones with modest bluntness, two and three-dimensional concave shapes, and some convex shapes at high angles of attack over a wide range of Mach number. However, for bodies with large bluntness, hyperballistic bodies of revolution, general convex shapes at low and moderate mean angle of attack, the assumption is not well satisfied, and Newton-Busemann theory would not be expected to provide a good approximation at conditions far removed from the strict Newtonian limit of $M_\infty \to \infty$ and $\gamma \to 1$. As a consequence of the requirement to reduce heat-transfer rates and to provide efficient payload packaging, such bodies are of considerable importance at hypersonic Mach numbers, and alternative prediction methods for relatively thick shock layers must be sought.

To remove some of the limitation of Newtonian theory caused by the requirement for an infinitesimal shock layer, Seiff[4] proposed the embedded Newtonian method. In this method, which was originally developed for steady flow, a nonuniform rotational inviscid flow is defined downstream of the bow shock wave, whose shape is determined by the nose shape and drag coefficient. The pressure on the afterbody embedded in this flowfield is calculated using generalized Newtonian theory. Physically, this method takes account of the large reductions in both dynamic pressure and velocity which arise in the entropy layer caused by the bow shock.

Ericsson[5] extended this concept to deal with unsteady flow problems, originally to determine the effects of the entropy gradient generated by the nose bluntness on the static and dynamic stability of an ablating flared body of revolution. Later Ericsson and Scholnick[13] and Ericsson[14] used the method to determine the effects of moderate hemispherical nose bluntness on the stability of slender cones, and Ericsson[15] extended the analysis to include large bluntness, moderate angles of attack and finite amplitude of oscillation. A more unified treatment of the unsteady embedded Newtonian method presented by Ericsson[16,17] removed the hypersonic Mach number restriction on the previous methods, so that the range of application for blunted slender cones could be extended down to $M_\infty = 3$. The earlier methods of predicting the stability of hemisphere-cylinder-flare bodies were extended by Ericsson[18] to include other more general hyperballistic shapes with different nose geometries, and to include the effect to Mach number down to moderate supersonic speeds.

Newton-Busemann theory, as described earlier and suitably modified to account for the pressure coefficient at the

stagnation point, provides reasonable estimates of pressure coefficients and stability derivatives only when the shock layer is very thin. It is also well known that the Busemann theory overestimates the centrifugal pressure correction term in steady flow with $\gamma = 1.4$ with the result, for example, that the pressure on a sphere is predicted to be zero at a position displaced 60 deg from the front stagnation point. This is at variance with the prediction of numerical calculations for $\gamma = 1.4$ and with experimental results, and suggests that when $\gamma \neq 1$ and the shock layer is not thin, the centrifugal pressure correction term for steady flow is overestimated. Moreover, Van Dyke[19] showed that modified Newtonian theory provides reasonable agreement with numerical predictions for cylinder and sphere flows at $M_\infty = \infty$, $\gamma = 1.4$ for angles up to at least 40 deg from the stagnation point, although this is purely fortuitous in that the effect of different γ appears to cancel the effect of the centrifugal correction term. Although conjectural, it is suggested that broadly similar effects occur with regard to the centrifugal term in respect to the streamline curvature resulting from nonsteady body motion, and it is possible that the change from $\gamma = 1.0$ in Newton-Busemann theory to $\gamma = 1.4$ for actual flows provides an effect of opposite sign and of the same order as the centrifugal term. It is, therefore, argued that for the thick shock layer flows at finite Mach number with $\gamma = 1.4$, characteristic of a large range of hypersonic shapes, the use of the straightforward modified Newtonian impact pressure may, on the same grounds as for steady flows, give a good approximation to the pressure in unsteady embedded Newtonian flow. For many hypersonic vehicles, the region in which the Newtonian-Busemann assumptions are most closely satisfied is close to the apex. For the remainder of the flowfield within the relatively thick shock layer, the assumptions are not well satisfied, and the flowfield is better approximated as that generated by a strong curved bow shock, whose shape is determined by nose geometry, together with an inviscid shear flow downstream of the shock in which the pressures are deduced using local generalized Newtonian concepts.

The dynamic pressure $\frac{1}{2}\rho V^2$ and local flow velocity V in the flowfield downstream of the shock are both expressed as functions of the dimensionless radial distance $R' (= R/d_N)$ (see Fig. 1) using the concept of similar profiles:

$$\frac{\rho V^2}{\rho_\infty V_\infty^2} = f^*\left(\frac{R'}{R'_s}\right) \tag{3a}$$

$$\frac{V}{V_\infty} = g^*\left(\frac{R'}{R'_s}\right) \tag{3b}$$

where R' is determined from Fig. 1 in terms of the vertical displacement $z' (= z/d_N)$ and angular displacement α. Reference 18 expresses f^* and g^* in terms of the parameter X^* defined by

$$X^* = \left(\frac{R' - 0.5}{R'_s}\right)^2 \tag{4}$$

for a variety of steady flows past bodies of different nose shapes. The empirical expression for f^* and g^* are arranged to provide close agreement with flowfield calculations based on the Method of Characteristics, for example, over a wide range of Mach numbers. Following Ericsson,[18] the functions employed for f^* and g^* are

$$f^*(X^*) = f_o + 2.75X^* \tag{5a}$$

$$g^*(X^*) = 1 - 0.362(1 - f_o)^{1/2} + 0.6X^{*0.5} \tag{5b}$$

noting that the maximum value of these functions should not exceed unity at the termination of the inviscid shear layer. The term f_o is of major significance since it is via this term that the finite Mach number dependence of the profiles within the shock shape is determined. For finite Mach number applications

$$f_o = 0.17 + \left(\frac{9.65}{M_\infty + 8.7}\right)^3 \tag{6}$$

The local pressure coefficient on the embedded body in the flowfield downstream of the bow shock is given by the local modified Newtonian expression as

$$C_p = C_{p_o} + C_\gamma C_{p_{\max}}\left(\frac{v_n}{V}\right)^2\left(\frac{\rho V^2}{\rho_\infty V_\infty^2}\right) \tag{7}$$

where C_{p_o} is the blast wave pressure coefficient generated downstream of the blunt nose that would exist on an embedded cylinder, and the second term is the additional pressure coefficient due to the local body shape embedded in the inviscid flowfield. $C_{p_{\max}}$ is the pressure coefficient at the stagnation point that modifies the Newtonian impact pressure, and v_n is the velocity component perpendicular to the local surface element. C_γ is an empirical coefficient[18] that provides an effective Mach number dependence for the Newtonian pressure coefficient.

For a body perturbed in pitch by an angle θ from its mean angle of attack α, and pitching at a rate q about an axis distant x_{CG} from the origin, an expression for v_n/V is obtained. From thereon the procedure is to substitute for (v_n/V) in Eq. (7) differentiate with respect to α and with respect to $(qL/2V_\infty)$ to obtain $(\partial C_p/\partial\alpha)$ and $\partial C_p/\partial(qL/2V_\infty)$. By multiplying by the distance from the oscillation axis and appropriately integrating around the body surface, expressions for the pitching moment stability derivatives are obtained. Ericsson[18] has also obtained an expression for the pitching stability derivative $C_{m_{\dot\alpha}}$, due to rate of change of angle of attack that is a consequence of the time lag between the motion of the blast-wave generator (the nose) and the resulting motion of the

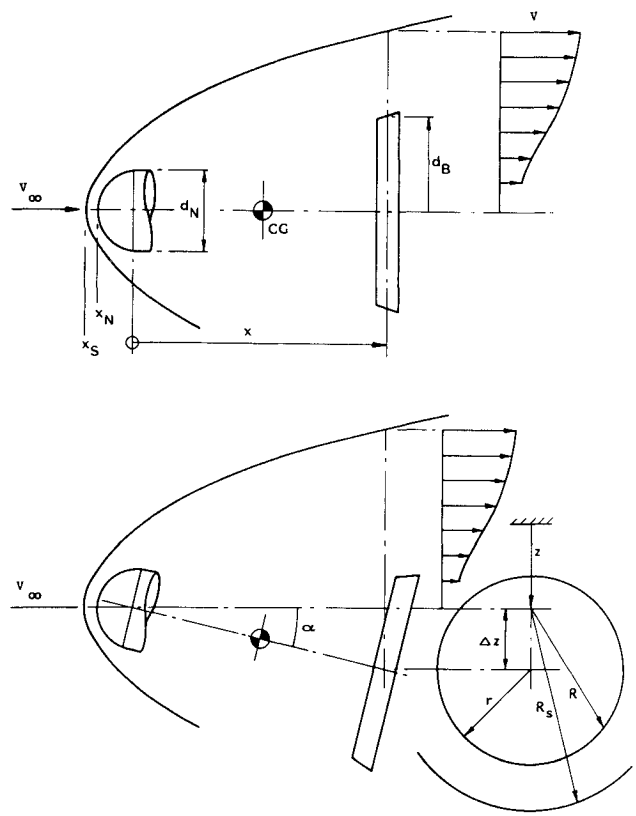

Fig. 1 Embedded flowfield and body geometry – adapted from Ericsson.[16]

inviscid shear layer at the body element. These procedures result in C_{m_α} and $C_{m_q} + C_{m_{\dot\alpha}}$ for the particular embedded body. Additional contributions to each of these derivatives from the nose portion, evaluated from Newtonian methods, are added to give the results for the complete shape.

In view of the success of Hui and Tobak's[20] unsteady Newton-Busemann flow theory as applied to bodies of revolution in providing results that are in agreement with the appropriate limiting results from gas dynamic theories, Tong and Hui[6] have applied Newton-Busemann flow theory to the embedded Newtonian flow concept described in the previous section. In essence, Tong and Hui have applied the centrifugal correction term to the expression used to calculate the pressure coefficient on embedded flares and compression surfaces within the flow downstream of the bow shock on a hemisphere cylinder basic shape. In their method they have preferred to use the value of 2 for the Newtonian coefficient rather than the value of $C_\gamma C_{p\max}$ used in Eq. (7), which provides better agreement with experimental results but is empirically based. The expression used by Tong and Hui,[6] therefore, is

$$C_p = C_{p_o} + 2\left(\frac{v_n}{V}\right)^2\left(\frac{\rho V^2}{\rho_\infty V_\infty^2}\right) + C_{p_c} \tag{8}$$

where C_{p_c} is the contribution to the pressure coefficient from the centrifugal term, and which has been calculated along similar lines to the method of Hui and Tobak.[20] The method, therefore, seeks to extend Seiff[4] and Ericsson's[18] embedded Newtonian concept so that, in the strict Newtonian limit the pressures on embedded surfaces would be calculated in a manner consistent with gas dynamic theories. For applications to finite Mach number flows, which is the essential purpose of embedded flow methods, empiricism is necessary to describe the similar profiles for the density and velocity variations downstream of the bow shock wave. For these Tong and Hui have used the following empirical fits to Seiff and Whiting[21] results for a hemisphere-cylinder in the high Mach number limit for hypersonic flight.

$$\frac{\rho}{\rho_\infty} = \begin{cases} 0.27 + 1.2X + 0.15X^2, & X \le 0.65 \\ 1, & X > 0.65 \end{cases}$$

$$\frac{V}{V_\infty} = \begin{cases} 0.7 + 0.3X^{1/2}, & X \le 0.65 \\ 1, & X > 0.65 \end{cases}$$

In the above, the parameter X [see Eq. (4), Ref. 7] is related to but slightly different in definition from X^* defined in Eq. (4). The expressions, employed by Tong and Hui[6] are Mach number dependent as a consequence of the Mach number dependence of the expressions used for the calculation of the bow shock wave shape in X, but do not, however, take into account the variations in the shape of the downstream flow profiles with Mach number that have been used by Ericsson.[18] It should be noted that in making subsequent comparisons between prediction methods and experimental results, it is difficult to draw conclusions with regard to the appropriateness of the embedded Newton-Busemann method vis-a-vis the unmodified embedded Newtonian method, since these inherent differences exist.

The inclusion of the centrifugal pressure correction within both steady and nonsteady contributions to the pressure coefficient should, therefore, improve the rigor of the embedded flow concept. However, in steady flow, Newton-Busemann theory gives poor comparison with experimental results, principally as a consequence of the finite-thickness shock layers that occur on the majority of hypersonic vehicles. It is one of the purposes of the present paper to compare both the uncorrected and the centrifugally corrected embedded Newtonian method with experimental results for stability derivatives in single-degree-of-freedom pitching motions. Such a comparison is difficult to make since the results published by Tong and Hui[6] incorporate Mach number dependence of the shock shape, but do not contain Mach number dependent functions for the downstream velocity and density profiles, whereas the centrifugally uncorrected embedded Newtonian results of the present paper do. Comparisons between the results of Ref. 6 and the embedded Newtonian results that are used to identify the magnitude of the centrifugal term have been facilitated by recalculating the results in the present paper with alternative forms of the equations that are appropriate for infinite embedded Mach numbers. However, it is noted that the experiments used for comparison have been performed at the relatively low hypersonic Mach number of 6.85 in which the joint $M \to \infty$, $\gamma \to 1$ assumptions are not well satisfied. Not only is the freestream Mach number relatively low, but the embedded flow Mach number is even lower, thus rendering simple Newtonian flow assumption even more inappropriate for the local Newtonian flow calculations on embedded surfaces.

Wind-Tunnel Facility, Techniques, and Models

The experiments were performed in the isentropic light piston tunnel (ILPT) at the University of Southampton.[22] This is an intermittent wind-tunnel facility providing an open jet test section of nozzle exit plane diameter 0.21 m with a flow Mach number of $M = 6.85$ for durations of typically 0.5 s. The unit Reynolds number test range available is approximately 7.5×10^6 m^{-1} to 40×10^6 m^{-1}.

The test procedure employed to determine the aerodynamic stiffness and damping derivatives is the small-amplitude free-oscillation technique. The model under test is held captive in the wind-tunnel open jet test section flow on a sting support. The model is mounted on an internally sited rotary flexure pivot that allows the model to oscillate in the pitch plane $\theta \sim \pm 1$ deg. The experimental data are obtained using the classical small-amplitude local linearization technique, applied about the equilibrium angle of attack. The center of rotation corresponds to the effective center of gravity location. The flexure pivot is mounted onto a rigid sting support, which is quadrant-mounted on the test section floor. Dynamic stability data obtained in such circumstances may be subject to support-interference effects unless certain sting design criteria are met. It is believed that the results presented herein are free from such interference in view of the following experimental features: the sting geometry is symmetric; the test Mach number is relatively low ($M = 6.85$); the parameter, visible sting length behind the model divided by model base diameter, is large – approximately 3; the negligible influence on these

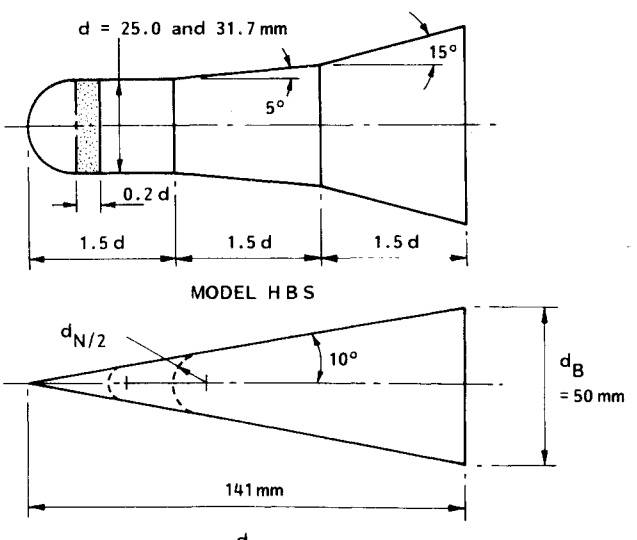

Fig. 2 Shapes tested for dynamic stability.

tests of base pressure effects has been previously demonstrated by open- and closed-model base results reported by East;[23] and finally, the sting support structure is of sufficient stiffness that the fundamental mode of vibration has frequencies at least two orders of magnitude higher than the model frequency. The reduced-frequency parameter for these experiments was $0.0018 < \omega' < 0.0092$.

The measurement of each pair of aerodynamic stiffness and damping derivatives necessitates two experimental tests, the so-called "wind-off" and "wind-on" runs. The ensuing model motions, both in vacuum (wind-off) and in the aerodynamic flow (wind-on), are monitored via an optical model tracking system[24] recorded and digitized for microcomputer storage. A subsequent analysis of the two-model motion time histories allows the aerodynamic pitch stability derivatives to be deduced. The experimental error bounds associated with the tests are of the order $C_{m_\alpha} \pm 2\%$ and $(C_{m_q} + C_{m_{\dot\alpha}} \pm 15\%$.

Experimental pitch stability data have been collected for the pointed and blunted 10 deg semiangle cones and the hyperballistic shape HBS shown in Fig. 2. These bodies were tested over a range of angles of attack $0 \le \alpha \le 16$ deg and axis oscillation positions.

Results and Discussion

Pointed and Blunted Cones

A 10 deg semiangle pointed cone has been investigated by East et al.[25] Small-amplitude, $\theta \simeq 1$ deg oscillatory experiments were performed, in the facility described earlier, at $M = 6.85$ in the Reynolds number range, $0.4 \times 10^6 < Re_b < 2 \times 10^6$. The zero angle-of-attack results showed how with increasing Reynolds number the stiffness derivative $-C_{m_\alpha}$ decreases in the range $1.0 \times 10^6 < Re_b < 1.4 \times 10^6$. A further increase in Reynolds number causes the stiffness derivative to rise to a value greater than the low Reynolds number value. This minimum of the stiffness derivative is accompanied by a maximum in the damping derivative $-(C_{m_q} + C_{m_{\dot\alpha}})$. Ward[26] reported a similar trend in pointed cone results, and showed how the maxima and minima in the respective derivatives occurred when there was transitional flow at the base of the model. These observations show that the results given in Fig. 3 are subject to a transitional aft body at $Re_b = 1.45 \times 10^6$ and subject to wholly turbulent aft body at $Re_b = 2.17 \times 10^6$. Recent surface thermographs have confirmed the transitional nature of the boundary layer at the rear of the pointed cone for these flow conditions. At the greater Reynolds number condition, the inviscid embedded Newtonian technique yields results similar to the experimental trend in that they are generally angle-of-attack-invariant in the range $0 \text{ deg} \le \alpha \le 16$ deg. It is likely that the increase in static stability above the theoretical prediction shown by the experimental data is due to boundary-layer displacement thickness effects.

Ericsson[27] has postulated that the angle-of-attack-dependent trends are associated with aft cone transitional flow. Increasing the angle of attack causes the windward surface transition location to move aft slightly; however, this movement is much less than the associated forward movement of the lee-side transition. With a moderate increase of the angle of attack the crossflow-enhanced lee-side transition location moves rapidly forward to remain fixed despite further increase in the angle of attack. This asymmetric transition point movement modifies the viscous contribution to stability. This is vividly shown by the comparison between the angle-of-attack-dependent, small-amplitude experimental data at $Re_b = 1.45 \times 10^6$ and the inviscid embedded Newtonian theory results shown by Fig. 3. In comparison with the inviscid theory, the $\alpha = 0$ deg experimental stability derivatives are consistent with the effects associated with aft body transition rear of the oscillation axis. The viscous moment contribution acts aft of the oscillation axis at $\alpha = 0$ deg; but, with increasing angle of attack, the viscous contribution moves forward to become a statically stabilizing effect for $\alpha > 5$ deg. This conclusion is drawn from a comparison with the inviscid, angle-of-attack-dependent theoretical results. The dominant influence is that of forebody crossflow ($\alpha \neq 0$ deg) that thickens the lee-side boundary layer. It is the authors' belief that the viscous influence responsible for the results observed is an interaction between transition and boundary-layer vortices whereby the prevailing boundary-layer state determines the different nature of the lee-side flow.

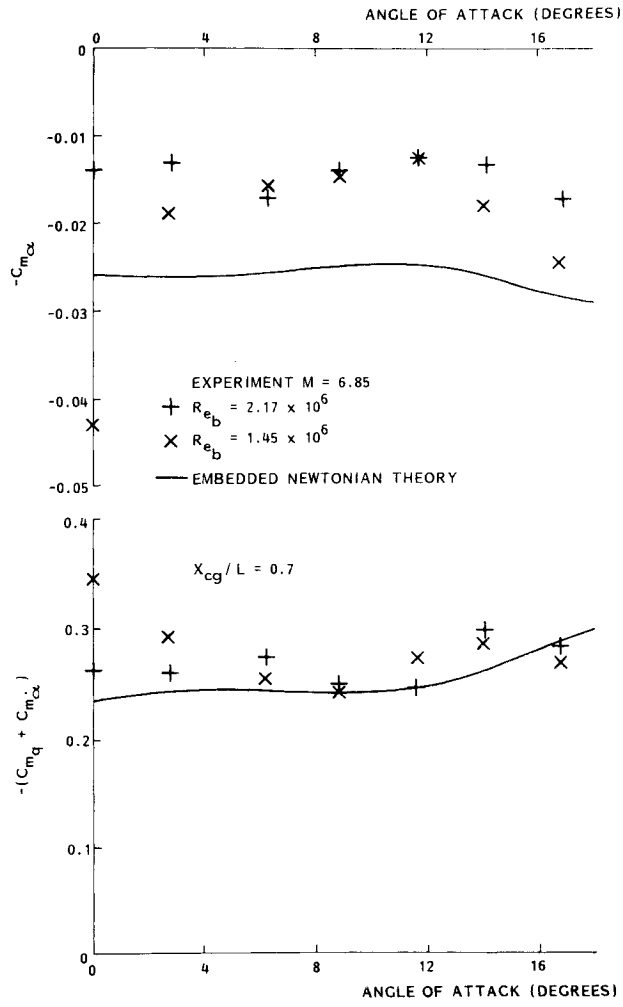

Fig. 3 Pitch stability derivatives vs angle of attack for a 10 deg semiangle pointed cone.

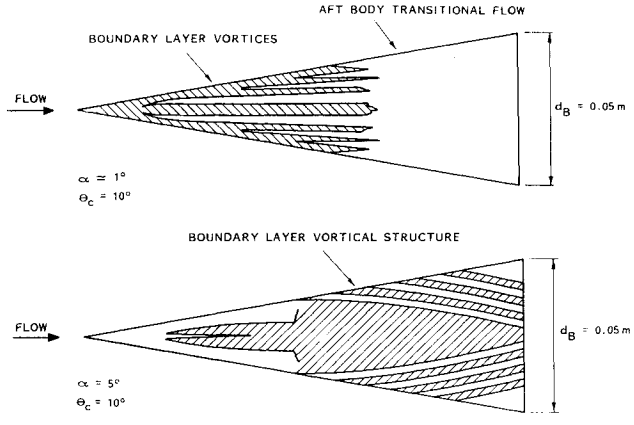

Fig. 4 Thermographic surface flowfield maps for a pointed cone, $M = 6.85$, $Re_b = 1.45 \times 10^6$.

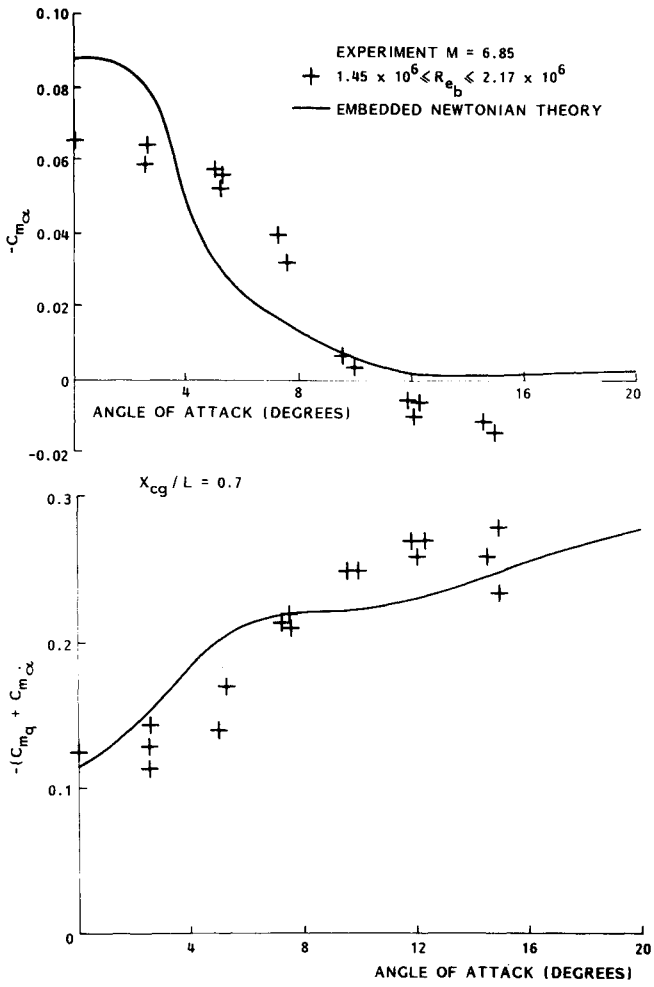

Fig. 5 Comparison of embedded Newtonian and experimental pitch stability derivatives vs angle of attack for a 0.2 bluntness ratio, 10 deg semiangle cone.

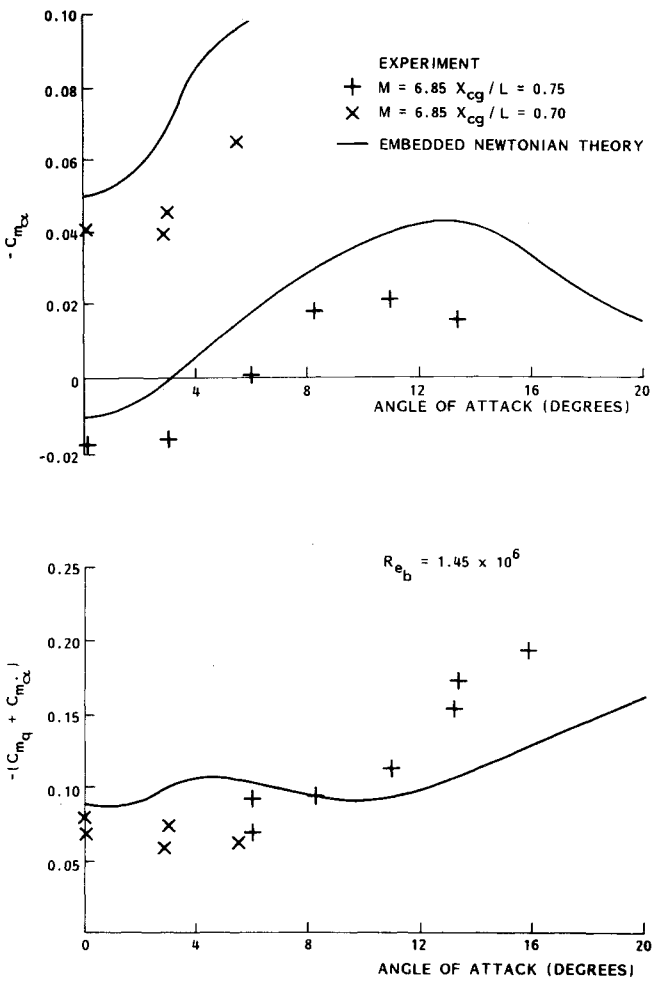

Fig. 6 Comparison of embedded Newtonian and experimental pitch stability derivatives vs angle of attack for a 0.4 bluntness ratio, 10 deg semiangle cone.

Figure 4 shows two sketches of surface flowfields revealed by liquid crystal thermographic methods. Figure 4a shows the lee-side flow with the model at $\alpha \simeq 1$ deg. It clearly shows the general high-temperature region for the aft one-third of the body associated with the transitional region. However, for the forward portion of the body, separate hot and cold regions are shown associated with a generally stream-wise vortical structure caused by the viscous crossflow. Results of further experiments show that this structure persists in a modified form at angles of attack up to at least 5 deg. Figure 4b identifies the flowfield at $\alpha \simeq 5$ deg, showing fundamental differences in fore and aft body vortical structure. This suggests that the former transitional flow persists not as a transitional flow per se, but as an influence on the nature of the aft body lee-side boundary-layer vortical structure.

Figures 5 and 6 show a comparison between the prediction of embedded Newtonian theory and experimental results for 10 deg semiangle cones with hemispherical nose bluntness 0.2 and 0.4, respectively. The experimental variations of the derivatives $-C_{m_\alpha}$ and $-(C_{m_q} + C_{m_{\dot\alpha}})$ with angle of attack are complex and very dependent on nose bluntness. Considerable nonlinear effects are demonstrated, and significant shifts of center of pressure are evident. Only the turbulent boundary-layer pointed cone derivative is relatively independent of angle of attack up to 20 deg (see Fig. 3).

The general trends of the stiffness derivative $(-C_{m_\alpha})$ are well predicted by embedded Newtonian theory. For the bluntness ratio of 0.2, the stiffness derivative $-C_{m_\alpha}$ decreases with angle of attack, indicating a forward shift of the center of pressure. This is accounted for in the theory by the forward movement of the minimum in the typical blunted cone blast wave induced pressure coefficient as angle of attack of the windward surface increases. Since the windward surface plays an increasingly dominant role as angle of attack increases, this forward movement of pressure distribution is reflected in the derivatives. The effect of bluntness on damping is to destabilize as bluntness is increased. This is due to the lower dynamic pressure acting on the conical surface due to the entropy layer resulting from the bow shock.

Data from small-amplitude longitudinal stability experiments performed on a 0.2 bluntness ratio 10 deg cone[23] at two Reynolds numbers, $Re_b = 1.45 \times 10^6$ and 2.17×10^6, show the results to be independent of Reynolds number within this range and for angles of attack $0 \text{ deg} \leq \alpha \leq 16$ deg. Nose bluntness produces a region of high-entropy flow, which reduces the local Reynolds number and which has been shown to delay transition.[28] As the equivalent pointed cone flow is transitional at the rear of the body for the experiments under discussion, the bluntness will serve to move transition off the body into the wake. The above implies that the blunted cone is subject to a purely laminar flow at the Reynolds numbers appropriate to these data. The trends shown by Fig. 5 identify the α-dependent viscous contribution to be statically stabilizing, but dynamically destabilizing for angles of attack $\alpha < 8$ deg. This trend reverses for angles of attack $\alpha > 8$ deg. The low angle-of-attack trend is thought to be a crossflow effect, which is known to be statically stabilizing when the load center of this effect is ahead of the center of gravity position. At approximately $\alpha = 8$ deg where $\alpha \approx \theta_c$, it is postulated that the lee-side vortical structures separate from the body surfaces.

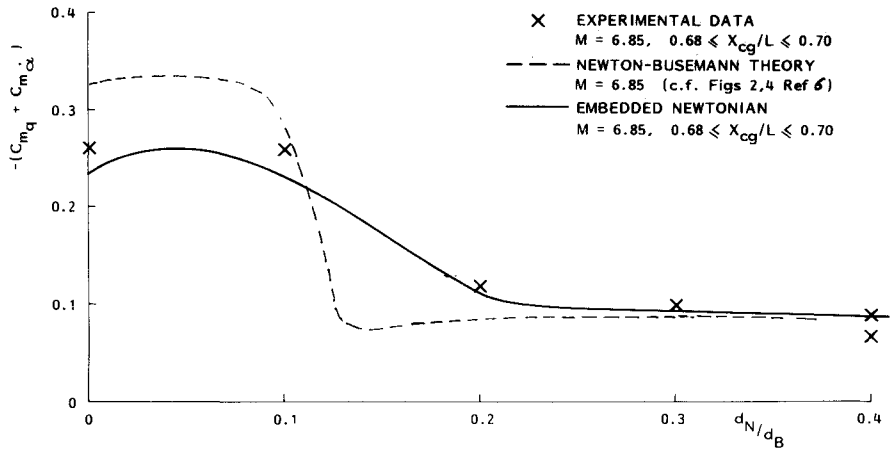

Fig. 7 Pitch damping derivatives results vs bluntness ratio for a family of 10 deg semiangle cones.

The leeward separated flows under discussion are revealed in schlieren flow visualization by embedded compression waves within the lee-side bow shock layer. The high angle-of-attack embedded flowfield is almost identical to the separated flows identified by Miller and Gnoffo[29] on the forecone of a blunted biconic geometry in a flow with $M = 6$ and $Re = 29 \times 10^6$ per meter.

The pitch stability derivatives at various angles of attack for 0.4 nose bluntness are shown on Fig. 6. Unlike the 0.2 bluntness ratio cone where the pressure field is composed of both nose and cone influences, the 0.4 bluntness ratio cone flowfield is dominated by the very large nose diameter. This causes a shift in center of pressure, which reduces the $\alpha = 0$ deg small-amplitude stability derivatives in comparison with the inviscid theory. This comparison implies that the entropy layer effects extend further downstream than the inviscid results would suggest. It is almost certain that both of these cones are subject to a purely laminar flow at the Reynolds number of the tests, $Re_b = 1.45 \times 10^6$. At increased angles of attack, the entropy layer present on the dominant windward surface thins. This has the effect of increasing the pressure on the aft region of the body. The resultant change in the moment is reflected by the increase in stiffness derivative in the angle-of-attack range 0 deg $< \alpha <$ 5 deg. Although not shown on these plots, further increase in the angle of attack brings the increased conic pressure component forward and ahead of the oscillation axis, and the stiffness consequently decreases. The embedded Newtonian theory overestimates the damping derivatives in the range $\alpha < 10$ deg, and fails to predict the large rise in damping derivative seen at angles of attack $\alpha > 10$ deg. This tends to confirm the entropy effects being larger than predicted, since an increase of the nose bluntness would produce decreased stiffness and damping derivatives.

In Fig. 7, absolute values of the damping derivatives $-(C_{m_q} + C_{m_{\dot{\alpha}}})$ are compared with the results of prediction methods, whereas in previous papers such comparisons have generally been made with values normalized with respect to the equivalent pointed cone damping predictions. On the previous basis, comparison between experiment and prediction can be obscured if the values taken for the pointed cone differ. The comparison presented in Fig. 7 indicates that for low values of nose bluntness, the centrifugally corrected embedded Newtonian method appears to overpredict aerodynamic damping in comparison with simple Newtonian and experimental results.

A detailed comparison between experimental data and various theoretical prediction techniques for the pitch damping derivative of a 10 deg, 0.3 bluntness ratio cone at Mach number $M = 6.85$ is shown in Fig. 8 using results reported by Tong and Hui.[6] The results of Ref. 6 show that the embedded Newtonian method underpredicts the stability derivative, and that inclusion of the centrifugal term $(-C_{m_{\dot{\theta}}})_c$ is necessary to attain values in keeping with experimental data. However, as

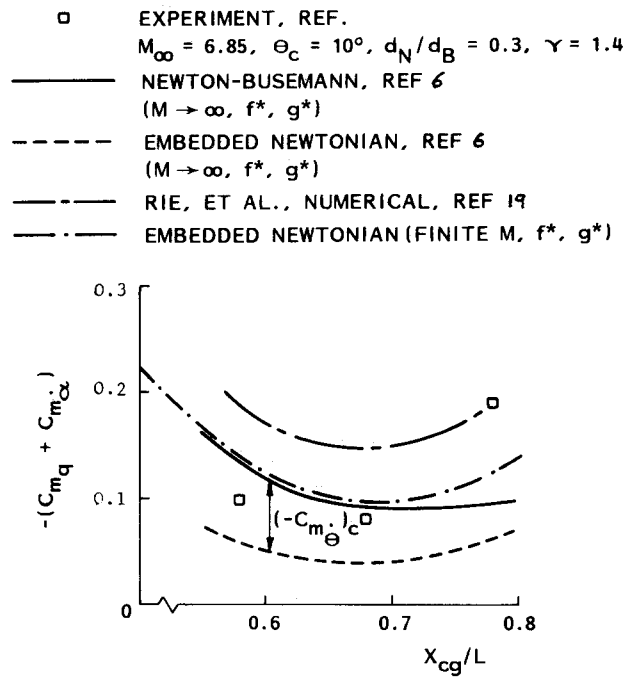

Fig. 8 Comparison between theoretical and experimental results of the pitch damping derivative vs oscillation axis position for a 0.3 bluntness ratio, 10 deg semiangle cone.

indicated earlier, it is noted that Tong and Hui's[6] embedded Newton-Busemann method employs infinite Mach number relations for the density and velocity profiles within the bow shock shear layer. If the functions, which have been shown for steady flow to be appropriate for finite Mach numbers, are used in the simple embedded Newtonian method, then the prediction is very similar to that with infinite Mach number functions f^* and g^* *with* centrifugal terms included. Indeed, it is arguably superior since the sensitivity to rearward axis position damping increasing is identified. This shows that with the appropriate finite Mach number functions applied to the embedded Newtonian method, the further inclusion of the centrifugal term would overpredict in comparison with experiment. It, therefore, appears that at the relatively low hypersonic Mach number at which the comparison has been made, adequate predictions are obtained by using embedded Newtonian methods without the Busemann correction. It must be acknowledged that this is a severe test of the Newton-Busemann concept that strictly applies in the $M \to \infty$, $\gamma \to 1$ limit, which is not well satisfied at the very low Mach numbers within the embedded flow on a blunt shape at $M = 6.85$.

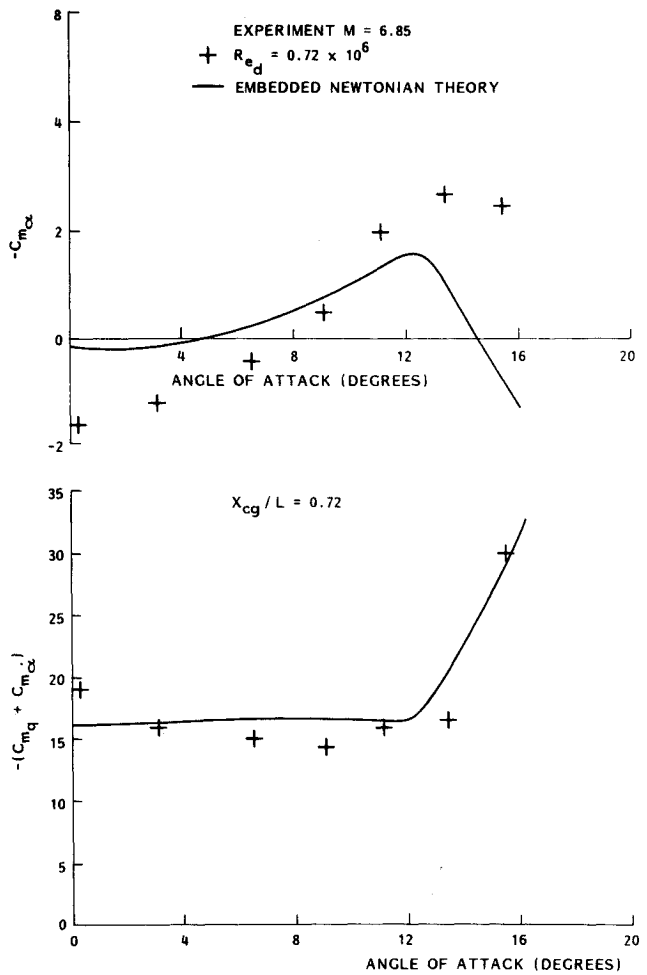

Fig. 9 Comparison of embedded Newtonian and experimental pitch stability derivatives vs angle of attack for the shape HBS.

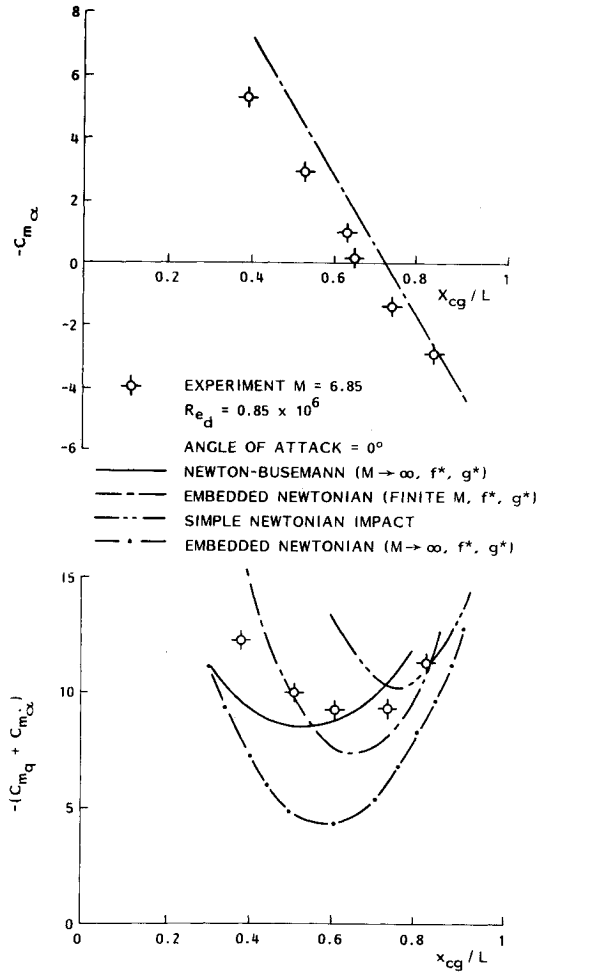

Fig. 10 Comparison between experimental and theoretical pitch stability derivatives results vs oscillation axis position for the shape HBS.

Hyperballistic Shape HBS

Data obtained for the aerodynamic stiffness and damping for the double-flared hemispherically blunted body HBS are shown in Figs. 9 and 10. The variations of the zero angle-of-attack values of $-C_{m_\alpha}$ and $-(C_{m_q} + C_{m_{\dot\alpha}})$ with the oscillation axis position are shown in Fig. 10. The center of pressure location, where $-C_{m_\alpha} = 0$, is predicted to be slightly further aft than experimentally observed, suggesting that embedded Newtonian theory slightly overestimates the double-flare effectiveness. Of the various prediction methods used for the aerodynamic damping $-(C_{m_q} + C_{m_{\dot\alpha}})$, embedded Newtonian with finite Mach number f^* and g^* functions [see Eq. (5)] shows the best agreement with experimental data. Simple modified Newtonian overpredicts the flare effectiveness and results in a damping minimum too far aft. Infinite Mach number functions used for f^* and g^* in the embedded Newtonian method result in a gross underprediction of the results. Tong and Hui's[6] prediction method effectively modifies this latter prediction by the addition of a centrifugal correction. The magnitude of the results is well predicted, but the damping minimum is shifted forward by some 15% of the body length, although it is unclear as to what contribution has been used for the damping contributed by the hemispherical nose in Tong and Hui's method. It could be argued that the addition of the centrifugal correction term to the embedded Newtonian method with the finite Mach number form of the embedded flowfield functions f^* and g^* would result in overprediction in comparison with the experimental data. Finally, it should be noted that the experimental test case ($M = 6.85$, $\gamma = 1.4$) provides an inappropriate source of comparison for a method that is strictly based on the $M \to \infty$, $\gamma \to 1$, Newton-Busemann theory limit.

Conclusions

A brief review of three analytical techniques for predicting the stability derivatives of slender axisymmetric hypersonic vehicles is presented. These techniques are Newtonian impact, embedded Newtonian, and embedded Newton-Busemann. Vehicle geometries considered are pointed and blunted 10 deg cones and a hyperballistic shape. Comparison of results from these prediction techniques with experimental data demonstrates that the embedded Newtonian technique provides a suitable method for approximate predictions of aerodynamic stiffness and damping over a wide range of conditions.

Although the centrifugal term of the embedded Newton-Busemann method is required for correct predictions in the regime of the limit $M = \infty$, $\gamma = 1$ where shock layers are thin, comparison with experimental results for a range of blunted cones and the hyperballistic shape HBS shows that prediction using this method at $M = 6.85$ provides no improvement over the less rigorous method in which the centrifugal correction is omitted.

It is noted that where flow structural change is present, in the form of transition and/or separation, viscous contributions to the stability derivatives cannot be ignored.

Acknowledgments

This work has been carried out with the support of the Procurement Executive, U.K. Ministry of Defence. The

authors wish to express their thanks to Mr. D. R. J. Baxter for his contribution to this paper. This paper is a précis version of a paper presented at the AGARD Symposium on *Aerodynamics of Hypersonic Lifting Vehicles*, Bristol, England, United Kingdom, April 6-9, 1987.

References

[1]Hayes, W. D. and Probstein, R. F., *Hypersonic Flow Theory 1*, Academic Press, New York, 1960.

[2]Zartarian, G., "Unsteady Airloads on Pointed Airfoils and Slender Bodies at High Mach Numbers," Wright Air Development Center, WADC TR-59-583, 1959.

[3]Busemann, A., *Handwörterbuck der Naturwissenschaften, IV*, Flüssigkeits und Gasbewegung, 2nd ed., Gustav Fisher, Jena, 1933, pp. 244-279.

[4]Seiff, A., "Secondary Flow Fields Embedded in Hypersonic Shock Layers," NASA TN D-1304, 1962.

[5]Ericsson, L. E., "Unsteady Aerodynamics of an Ablating Flared Body of Revolution Including Effects of Entropy Gradient," *AIAA Journal*, Vol. 6, Dec. 1968, pp. 2395-2401.

[6]Tong, B. G. and Hui, W. H., "Unsteady Embedded Newton-Busemann Flow Theory," *Journal of Spacecraft and Rockets*, Vol. 23, March-April 1986, pp. 129-135.

[7]Tobak, M. and Wehrend, W. R., "Stability Derivatives of Cones at Supersonic Speeds," NACA TN 3788, 1956.

[8]Cole, J. D., "Newtonian Flow for Slender Bodies," *Journal of Aerospace Sciences*, Vol. 24, 1957, pp. 448-455.

[9]Hui, W. H., "On Axisymmetric and Two-Dimensional Flow with Attached Shock Waves," *Acta Astronautica*, Vol. 18, Jan. 1973, pp. 35-44.

[10]Mahood, G. E. and Hui, W. H., "Remarks on Unsteady Newtonian Flow Theory," *Aeronautical Quarterly*, Vol. 27, Feb. 1976, pp. 66-74.

[11]Hui, W. H., "Stability of Oscillating Wedges and Caret Wings in Hypersonic and Supersonic Flows," *AIAA Journal*, Vol. 7, Aug. 1969, pp. 1524-1530.

[12]Scott, C. J., "A Theoretical and Experimental Determination of the Pitching Stability Derivatives of Cones in Hypersonic Flow," Univ. of Southampton, Hants, England, UK, AASU Rept. 267, 1967.

[13]Ericsson, L. E. and Scholnick, I. M., "Effect of Nose Bluntness on the Hypersonic Unsteady Aerodynamics of Flared and Conical Bodies of Revolution," *Journal of Spacecraft and Rockets*, Vol. 6, March 1969, pp. 321-324.

[14]Ericsson, L. E., "Universal Scaling Laws for Hypersonic Nose Bluntness Effects," *AIAA Journal*, Vol. 7, Dec. 1969, pp. 2222-2227.

[15]Ericsson, L. E., "Effect of Nose Bluntness, Angle of Attack, and Oscillation Amplitude on Hypersonic Unsteady Aerodynamics of Slender Cones," *AIAA Journal*, Vol. 9, Feb. 1971, pp. 297-304.

[16]Ericsson, L. E., "Unsteady Embedded Newtonian Flow," *Acta Astronautica*, Vol. 18, No. 5, 1973, pp. 309-330.

[17]Ericsson, L. E., "Generalized Unsteady Embedded Newtonian Flow," *Journal of Spacecraft and Rockets*, Vol. 12, Dec. 1975, pp. 718-726.

[18]Ericsson, L. E., "Hyperballistic Vehicle Dynamics," *Journal of Spacecraft and Rockets*, Vol. 19, Nov.-Dec. 1982, pp. 496-505.

[19]Rie, H., Linkiewicz, E. A., and Bosworth, F. D., "Hypersonic Dynamic Stability, Part III, Unsteady Flow Field Program," U.S. Air Force Flight Dynamics Laboratory, Wright-Patterson AFB, OH, FDLTDR-64-149, Pt. II, 1967.

[20]Hui, W. H. and Tobak, M., "Unsteady Newton-Busemann Flow Theory Part II – Bodies of Revolution," *AIAA Journal*, Vol. 19, Oct. 1982, pp. 1272-1273.

[21]Seiff, A. and Whiting, E. C., "Calculation of Flow Fields from Bow-Wave Profiles for the Downstream Region of Blunt-Nosed Circular in Axial Hypersonic Flight," NASA TN-D-1147, 1961.

[22]East, R. A. and Qasrawi, A. M. S., "A Long Stroke Isentropic Free Piston Hypersonic Wind Tunnel," Aeronautical Research Council, UK, R&M 3844, 1978.

[23]East, R. A., "Non-Linear Hypersonic Static and Dynamic Stability of Axisymmetric Shapes," Euromech Colloquium 126, Berlin, 1980.

[24]Hutt, G. R. and East, R. A., "Optical Techniques for Model Position Measurement in Dynamic Wind Tunnel Testing," *Measurement and Control*, Vol. 18, March 1985, pp. 99-101.

[25]East, R. A., Qasrawi, A. M. S., and Khalid, M., "An Experimental Study of the Hypersonic Dynamic Stability of Pitching Blunt Conical and Hyperballistic Shapes in a Short Running Time Facility," NATO AGARD CP-235, 1978.

[26]Ward, L. K., "Influence of Boundary Layer Transition on Dynamic Stability at Hypersonic Speeds," *Transactions of the 2nd Technical Workshop on Dynamic Stability Testing*, Arnold Air Force Station, TN, Paper 6, 1965.

[27]Ericsson, L. E., "Transition Effects on Slender Vehicle Stability and Trim Characteristics," *Journal of Spacecraft and Rockets*, Vol. 11, Jan.-Feb. 1974, pp. 3-11.

[28]Softley, E. J., Graber, E. C., and Zempel, R. C., "Experimental Observations of Transition of the Hypersonic Boundary Layer," *AIAA Journal*, Vol. 7, Feb. 1969, pp. 257-263.

[29]Miller, C. G. and Gnoffo, P. A., "An Experimental Investigation of Hypersonic Flow Over Bionics at Incidence and Comparison to Prediction," AIAA Paper 82-1382, 1982.